Materials Advances

ROYAL SOCIETY OF CHEMISTRY

PAPER

View Article Online
View Journal | View Issue

Cite this: *Mater. Adv.*, 2025, 6, 9590

Flexible fabric-integrated PAAm–LiCl hydrogel pressure sensor for wearable and soft robotics applications

Liza Liza,[a] Md Homaune Kabir,[a] Mohashin Kabir,[a] Md Nuramurtada Rafi,[a] Xu Ruidong,[a] Md Ashikur Rahman,[a] Tarikul Islam *[bc] and Tian Mingwei*[a]

This work presents the successful development of a flexible, fabric-integrated pressure sensor based on a woven cotton substrate and a polyacrylamide–LiCl (PAAm–LiCl) plain ionic hydrogel, synthesized *via* free-radical polymerization. The composite sensor was fabricated by uniformly coating the hydrogel onto woven fabric electrodes, forming an ionic conductive network capable of capacitive pressure sensing. A comprehensive series of characterizations confirmed the performance of the sensor and material integrity. Scanning electron microscopy (SEM) revealed a densely microporous surface structure that promotes enhanced ion transport. Fourier transform infrared (FTIR) spectroscopy confirmed the presence of characteristic O–H, C=O, and C–O functional groups, indicating hydrogen bonding, water retention, and the integration of polyacrylamide and cellulose components. Thermogravimetric analysis (TGA) demonstrated excellent thermal stability with major decomposition occurring at elevated temperatures, validating the robustness of the composite under thermal stress. Mechanical testing confirmed the strong self-adhesive properties of the material across diverse substrates, thereby improving its versatility for integration in practical applications. The pressure-sensing performance was validated through sensitivity analysis, dynamic and static gradient pressure response, frequency response under cyclic loading, and durability testing over 10 000 cycles. The sensor displayed rapid response and repeatability under varying pressure and frequency conditions, confirming its reliability and long-term functionality. These results collectively demonstrate the effective synthesis and integration of PAAm–LiCl hydrogel with woven fabric, leading to a stable, sensitive, and thermally durable pressure sensor. The developed system holds significant potential for use in wearable electronics, soft robotics, healthcare monitoring, and interactive human–machine interface technologies.

Received 21st August 2025,
Accepted 11th October 2025

DOI: 10.1039/d5ma00942a

rsc.li/materials-advances

1. Introduction

Hydrogels are soft, water-swollen polymeric materials that have gained remarkable global attention due to their unique ability to retain large amounts of water while maintaining a solid-like structure.[1,2] Since their first introduction by Wichterle and Lím in 1960, hydrogels have evolved into one of the most researched and applied biomaterials worldwide, consistently ranking among the top materials in biomedical and wearable electronics research.[3] Widely used in drug delivery, wound healing, contact lenses, and tissue engineering, the public often perceives hydrogels as purely medical or cosmetic materials.[4–6] However, recent advances have reshaped this perception, positioning hydrogels as multifunctional smart materials capable of responding to external stimuli such as pressure, strain, or temperature.[7,8] This growing interest has inspired researchers to explore the integration with flexible electronics and textiles, aiming to create innovative devices like wearable sensors and artificial skins.[9]

The unique performance of hydrogels originates from their structural characteristics—particularly the nature of their cross-linking mechanisms, which can be physical (supramolecular) or chemical (covalent).[10,11] Chemically cross-linked hydrogels are known for their mechanical strength and durability, while physically cross-linked variants provide reversible properties and responsiveness to external stimuli such as temperature, pH, or stress.[10,12] These networks have been tailored into ionically conductive hydrogels, which exhibit impressive mechanical properties—such as tensile strength reaching

[a] College of Textiles and Clothing, Qingdao University, Qingdao 266071, China. E-mail: mwtian@qdu.edu.cn
[b] Department of Textiles, Merchandising, and Interiors, University of Georgia, Athens, GA 30602, USA. E-mail: tarikul@uga.edu
[c] Department of Textile Engineering, Jashore University of Science and Technology, Jashore 7408, Bangladesh

1.66 MPa and elongation up to 849%—making them suitable for dynamic sensing applications.[13] However, traditional hydrogels still face notable challenges: low conductivity at sub-zero temperatures, limited fatigue resistance, and mechanical brittleness.[14,15] To overcome these issues, recent strategies such as the inclusion of nanofillers (*e.g.*, silver nanoparticles, carbon nanotubes, graphene oxide), the incorporation of antifreeze agents, and dual-network designs have been employed to enhance functionality, durability, and conductivity.[16,17] These modifications enable hydrogels to function as effective sensors for strain and pressure with high sensitivity and reliability.[18]

Among the various integration approaches, combining hydrogels with textile substrates—particularly woven fabrics—has demonstrated substantial promise in improving the performance of hydrogel-based sensor systems.[19] Compared with other textile forms, woven fabrics offer a more stable foundation for hydrogel-based sensors. Knitted fabrics, while highly elastic and comfortable, are prone to large deformations under stress, which leads to unstable sensor calibration and signal drift during repeated loading–unloading cycles.[20] Non-woven fabrics, on the other hand, provide good air permeability but their loosely bonded fibers lack sufficient structural integrity, resulting in reduced reproducibility of pressure responses and weaker hydrogel adhesion.[21] In contrast, woven fabrics exhibit high dimensional stability, minimal deformation, and strong interfacial bonding with hydrogel matrices, making them more reliable for repeated sensing operations. Their inherent porosity promotes strong interfacial bonding with hydrogels, facilitating better load transfer and enhanced signal detection.[22] In particular, the S-twill woven cotton fabric with an areal density of 140 GSM (grams per square meter) was chosen in this work because its regular twill weave pattern provides superior load-bearing capability and uniform stress distribution, while the medium weight ensures mechanical robustness without compromising flexibility. These characteristics collectively contribute to enhanced sensor stability, repeatability, and comfort, positioning S-twill woven cotton as an optimal substrate for fabric-integrated hydrogel pressure sensors.[23] Integrating plain hydrogel within such fabrics expands the application spectrum of these materials, offering potential solutions for smart garments, physiological monitoring, and therapeutic wearables.[24–26]

Hydrogel-based pressure sensors operate on the principle of converting mechanical deformation into detectable electrical signals through mechanisms such as resistance variation, capacitance modulation, or changes in ionic conductivity.[27,28] Plain hydrogels, when modified with conductive agents or embedded in conductive frameworks, can serve as highly sensitive pressure sensors.[29] Techniques such as incorporating silver nitrate, graphene, or nickel-coated yarns into the sensor matrix allow the detection of minimal pressure changes with great precision.[30,31] For instance, Xiao Rui Ye *et al.* reported a textile-only capacitive sensor using graphene nanoplatelets and nickel-coated woven fabric electrodes, achieving a pressure sensitivity of 0.38 kPa^{-1} and a detection threshold of just 1.23 Pa.[32] In another study, cotton non-woven alginate conductive hydrogel was synthesized using the sol–gel method. Different concentrations of sodium alginate (0.5%, 1%, and 1.5%) and silver nitrate (0.5%, 10%, and 15%) were used to investigate their impact on the performance of the conductive hydrogel and were characterized through FTIR, SEM, and XRD, confirming their effective pressure sensitivity and conductivity.[9] These studies reinforce the feasibility of constructing flexible, low-cost, and high-performance pressure sensors by integrating hydrogels with fabric substrates.[33,34] Although many of these sensors incorporate complex fillers and layering, limited research has addressed plain, filler-free hydrogel systems in combination with fabric substrates, which is valuable for cost-effective and scalable development.[26,35] However, plain hydrogel-based sensors often face performance bottlenecks, including low sensitivity and slow response times, primarily due to their limited ionic conductivity. Recent studies have demonstrated that regulating ion concentration within the hydrogel network by introducing salts such as LiCl or NaCl can effectively enhance ionic mobility, thereby improve conductivity and reducing response times.[36,37] Building on this approach, the present work employs a plain PAAm–LiCl hydrogel, which not only reduces material and fabrication costs but also addresses these fundamental limitations by leveraging the ion-regulating effect of LiCl.[38]

Despite these advancements, several research gaps remain. Many hydrogel-based sensor systems rely on costly conductive materials, intricate multi-layered fabrication processes, and rigid base structures, which limit their accessibility and scalability.[39,40] There is a distinct lack of studies focusing on plain hydrogel systems embedded in untreated woven fabrics, which could significantly reduce production complexity and cost.[41–43] Additionally, systematic comparisons between basic hydrogel-fabric composites and nanomaterial-enhanced systems are scarce, hindering our understanding of practical performance *versus* cost-efficiency. These challenges have motivated the current study, which aims to develop a simple, low-cost, woven fabric-based pressure sensor using plain hydrogel without additional conductive fillers. By optimizing hydrogel formulation and textile structure, this research seeks to demonstrate that high sensitivity and flexibility can be achieved without complex modifications.[43,44] This approach opens doors to future innovations such as wireless hydrogel sensor systems, thermally stable smart garments, and eco-friendly wearable healthcare platforms. Future research directions may also include enhancing environmental adaptability, improving biodegradability, and integrating multifunctional sensing capabilities for broader industrial and medical applications.

2. Materials

Acrylamide (AAM, ≥90%, monomer) and lithium chloride (LiCl, ≥99%) were purchased from Shanghai Aladdin Reagent Co., Ltd. *N*,*N*′-methylenebisacrylamide (MBAA, 99%, crosslinking agent) and ammonium persulfate (APS, ≥98%, thermal initiator) were obtained from INNOCHEM. *N*,*N*,*N*′,*N*′-Tetramethyl ethylenediamine (TEMED, ≥99%, accelerator)

was purchased from ALFA. All chemicals were of analytical grade and used without further purification. Deionized (DI) water was used as the solvent in all experiments. The woven fabric substrate used in the sensor fabrication was commercially sourced *via* the Taobao online platform. S-twill woven fabric with 140 GSM (grams per square meter) was selected the experiment and investigated the mechanical durability, flexibility, and compatibility with hydrogel integration for pressure sensing applications.

2.1. Experimental methods

2.1.1. Preparation of ionic plain hydrogel. The preparation of the ionic plain hydrogel was carried out following modified procedures based on previously reported methods for thermally polymerized conductive hydrogels.[45] Initially, 2.11 mol of acrylamide (AAM, monomer) and 2.00 mol of lithium chloride (LiCl, conductive salt) were co-dissolved in deionized water under continuous stirring using a constant-temperature magnetic stirrer. The solution was stirred for 30 minutes at ambient temperature to ensure complete dispersion of the components. Subsequently, 0.0040 g of *N*,*N*′-methylenebisacrylamide (MBAA, crosslinking agent) and 0.0070 g of ammonium persulfate (APS, thermal initiator) were added to the solution. After complete dissolution of the crosslinker and initiator, 15 μL of *N*,*N*,*N*′,*N*′-tetramethyl ethylenediamine (TEMED, accelerator) was introduced to initiate polymerization. The resulting precursor solution was immediately poured into prefabricated acrylic molds and subjected to thermal polymerization at 80 °C for 20 minutes.

Through this thermal process, a conductive polyacrylamide–LiCl-based ionic plain hydrogel was successfully synthesized. During polymerization, the acrylamide monomers (C_3H_5NO) undergo free-radical polymerization to form polyacrylamide chains $(C_3H_5NO)_n$, with the presence of LiCl enabling ionic conductivity within the hydrogel matrix. The thermal energy facilitated efficient network formation, yielding a uniform, gel-like material suitable for integration into pressure sensing applications, as illustrated in Fig. 1a and b.

2.1.2. Fabrication of woven fabric electrode with plain ionic hydrogel. The sensing mechanism of the woven fabric–hydrogel system is governed by the formation of an electric double layer (EDL) at the hydrogel–electrode interface (see Fig. 1c).

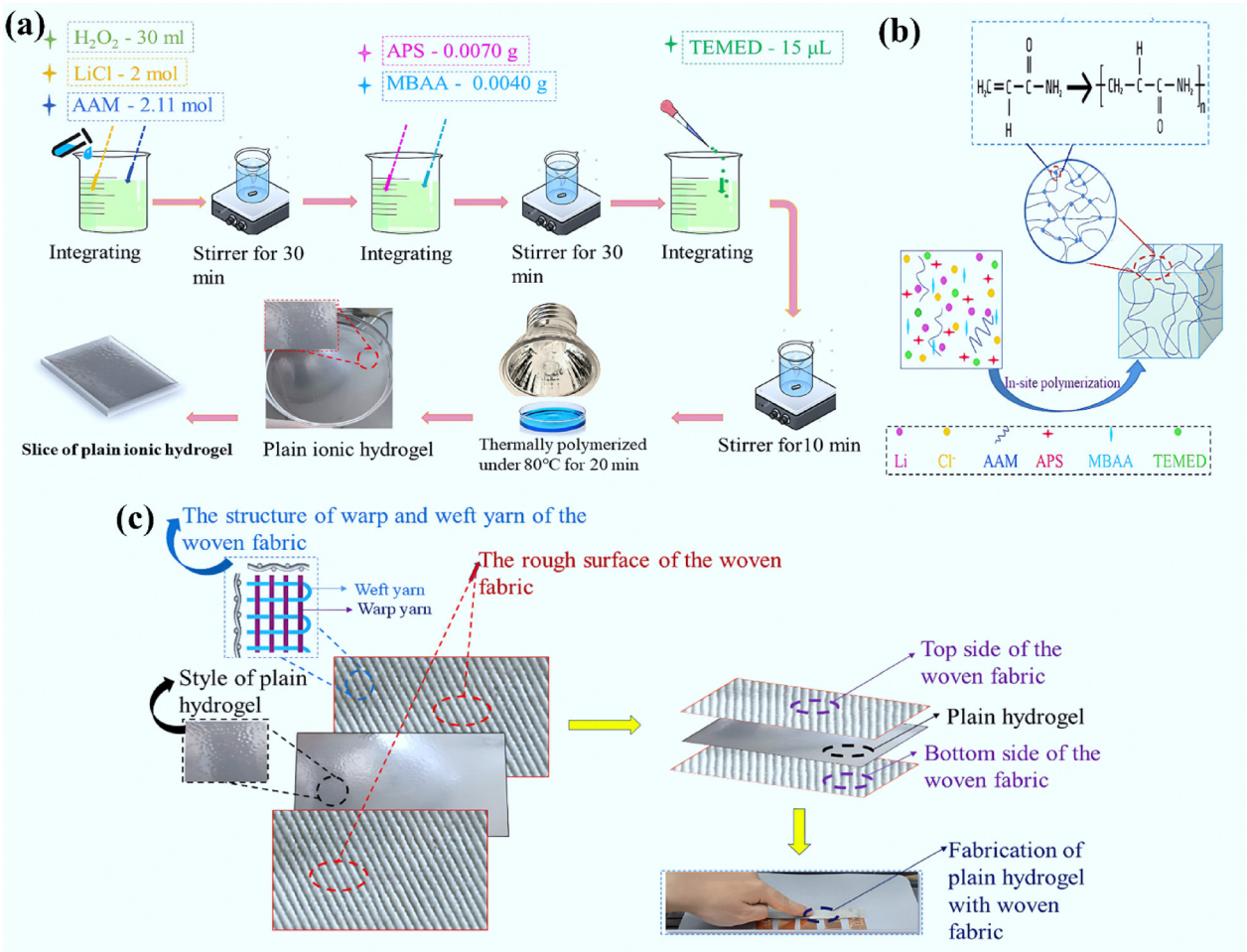

Fig. 1 (a) Thermal polymerization process of the polyacrylamide–LiCl (PAAM–LiCl) for ionic plain hydrogel; (b) filling layer by the thermal polymerization process of the PAAM–LiCl hydrogel; (c) fabrication process of ionic plain hydrogel with woven fabric electrode.

The woven fabric electrodes possess a microscopically rough surface composed of warp and weft yarns, which provides multiple micro-asperities for hydrogel contact. In the initial unloaded state, the hydrogel conforms to these asperities, generating a baseline EDL capacitance due to the interfacial accumulation of mobile ions (Li^+ and Cl^-) from the hydrogel and compensating charges on the fabric electrode surface.

When external pressure is applied, two key processes occur simultaneously: (i) the effective contact area between the hydrogel and electrode increases as the hydrogel is compressed into the inter-yarn gaps, and (ii) the interfacial distance between the ionic charges in the hydrogel and the electrode surface decreases. Both effects contribute to an increase in the interfacial charge density and a corresponding rise in EDL capacitance. The sensitivity ($GF_1 = 0.076\ kPa^{-1}$ and $GF_2 = 0.029\ kPa^{-1}$) reflects the magnitude of this pressure-induced modulation. However, because the rough woven surface already provides a relatively high baseline contact area in the unloaded state, the creation of additional new contact sites under pressure is limited. This explains the comparatively lower sensitivity compared to multilayer or nanostructured electrodes, where the variation in contact points under deformation is more pronounced.

Upon release of pressure, the elastic recovery of the PAAm–LiCl hydrogel restores the initial contact configuration, allowing ions to redistribute rapidly and thereby ensuring repeatable capacitance changes over multiple cycles. This reversible EDL-based mechanism underpins the stable operation of the sensor, while the integration of a plain hydrogel with a woven fabric electrode provides a low-cost and filler-free strategy without compromising durability or responsiveness.[28]

3. Characterization

3.1. Surface morphology

The surface characteristics of the conductive polyacrylamide–LiCl (PAAM–LiCl) ionic hydrogel e-textile were analyzed using a TESCAN VEGA3 (Gzech) scanning electron microscope (SEM) with an accelerating voltage set at 10 kV. The SEM images, taken with a scale of 200 μm, revealed a compact microporous structure along with significant surface roughness. Before imaging, the samples were sputter-coated with a 30 nm thick gold (Au) layer to enhance surface conductivity and prevent charging effects during observation.

3.2. Sensitivity and gauge factor

The sensitivity of the pressure sensor, made from a transparent and flexible polyacrylamide-alginate double network hydrogel fiber, was assessed by calculating its gauge factors (GF) under varying conditions. The sensitivity of the sensor was evaluated by measuring the relative change in resistance in response to varying applied pressures (or strains), and, calculated using eqn (1).

$$GF = (\Delta C/C_0)/\Delta P \quad (1)$$

where ΔC is the change in capacitance, C_0 is the initial capacitance without applied pressure, and ΔP is the change in applied pressure. This equation reflects how sensitively the sensor converts mechanical pressure into electrical signals.

The performance of the sensor was evaluated across a broad pressure detection range of 0 to 300 kPa, illustrating its ability to sense both low and high-pressure inputs. These findings validate the impressive sensitivity and potential of the sensor for a wide range of pressure-sensing applications.

3.3. Response time analysis

The dynamic response of the sensor was assessed by applying and releasing a sudden mechanical stimulus, while recording the real-time resistance change. Response time was defined as the time to reach 90% of the peak signal, and recovery time as the return to 10% of the baseline. Measurements were conducted at room temperature. These efficient response and recovery features highlight the appropriateness of the sensor for applications that demand real-time and precise pressure monitoring.

3.4. Dynamic frequency response

The performance of the sensor was tested at the same pressure but with different input frequencies: 1 Hz, 2 Hz, and 4 Hz. The results showed stable and distinguishable output signals at each frequency, suggesting the sensor is suitable for dynamic environments where the rate of pressure application may vary.

3.5. Stability and durability

A cyclic test was conducted by subjecting the sensor to 10 000 repeated pressure cycles (0–10 kPa) to assess its durability and mechanical stability. The results demonstrated excellent repeatability and long-term operational stability, making them effective for both industrial and wearable applications.

3.6. Gradient pressure (dynamic and static)

The performance of the sensor under gradient pressure was evaluated by applying both static and dynamic pressures in a stepwise manner. For static tests, different pressure levels (30 kPa, 60 kPa, 80 kPa, 110 kPa, and 160 kPa) were applied incrementally and held for a fixed duration to record the steady-state resistance response. For dynamic tests, cyclic pressures of varying magnitudes were applied to observe the real-time response and recovery behavior. The relative change in resistance was recorded at each pressure level to assess sensitivity and stability.

3.7. Pressure gauge

To apply controlled and calibrated pressure levels to the sensor. LCR Meter (inductance-capacitance-resistance meter) to record the real-time capacitance changes during pressure application and thus monitor sensor output. The pressure gauge of the sensor was measured using an LCR digital bridge tester (ECA200A, Creek Valley Polymer Technology Co., Ltd, Beijing, China) at a 200 kHz frequency with a 1 V AC signal. These instruments ensured precise pressure application and accurate signal measurement, enabling thorough characterization of the performance of the sensor.

3.8. Fourier transform infrared radiation

Fourier transform infrared spectroscopy (FTIR) analysis was conducted using a Bruker TENSOR27 model to identify the molecular structures based on characteristic absorption peaks. Each sample was scanned in the range of 500–4000 cm^{-1} at a resolution of 4 cm^{-1}, with 32 scans averaged per spectrum to improve the signal-to-noise ratio. The experiment was conducted at room temperature, and background spectra were collected prior to each scan to ensure accuracy.

3.9. Thermal analysis (TGA)

Thermogravimetric analysis (TGA) was performed using the STA449 F3 Jupiter analyzer to evaluate the thermal stability of hydrogels combined with woven and knit fabrics. A sample weight of 3–5 mg was heated from 30 °C to 800 °C at a rate of 10 °C min^{-1} under a controlled atmosphere. The weight loss was recorded as a function of temperature to evaluate the thermal stability and decomposition behavior of the samples.

3.9.1. Mechanical strength testing. Mechanical properties of both plain and patterned hydrogels were measured using a tensile strength tester (INSTRON 3365, USA). Test samples measured 4 cm in length, 1 cm in width, and 0.5 cm in thickness, with a gauge length of 2.9 cm. Tensile tests were performed at a speed of 10 mm min^{-1} to assess the strength and elasticity of the hydrogel.

4. Result and discussion

4.1. Scanning electron microscope (SEM)

The surface morphologies of the synthesized ionic hydrogel and the untreated woven fabric were analyzed using scanning electron microscopy (SEM), as shown in Fig. 2. These images offer valuable insights into the internal structure and compatibility between the hydrogel and textile substrate, which are essential for optimizing pressure sensing performance.

Fig. 2a illustrates the SEM image of the ionic plain hydrogel. The surface displays a dense, interconnected porous network with pore diameters predominantly in the range of 50–200 μm, based on the provided scale.[46] These large, open pores are characteristic of highly swollen hydrogel systems, where water content and flexibility of the polymer result in expanded microchannels. The porous architecture enhances the contact area between water molecules and the hydrophilic functional groups (*e.g.*, $-CONH_2$) of polyacrylamide, thereby supporting high ionic conductivity.[47] Furthermore, this structure allows the hydrogel to deform easily under pressure, a property essential for generating reliable pressure signals in soft sensor applications.

Fig. 2b presents the SEM image of the untreated woven fabric. The image reveals a fibrous structure consisting of intertwined cellulosic yarns with fiber bundle widths ranging from approximately 100–200 μm, consistent with typical cotton yarns.[48] The surface of the fibers appears rough, with evident microfibrillar delamination and irregular edges. These microstructural features not only increase the surface area but also improve the physical interlocking between the hydrogel and the fabric. The natural porosity between yarns facilitates penetration of the hydrogel into the textile matrix, contributing to enhanced mechanical anchoring and reduced delamination during deformation.[49] Both the hydrogel and the woven fabric exhibited compatible morphological features within a similar size range (up to 200 μm), enabling effective interfacial bonding, improved ion transport, and stable mechanical performance under compressive loads—key parameters for efficient hydrogel-based pressure sensors.

4.2. Sensor performance evaluation

4.2.1. Response time analysis. The response time of a pressure sensor reflects how quickly it reacts to an applied mechanical stimulus, which is critical for real-time sensing. As shown in Fig. 3a, the response curve of the hydrogel-based capacitive sensor indicates a sharp rise in the capacitance ratio ($\Delta C/C_0$) upon pressure application.[50] The interval between the start of pressure loading and the plateau region defines the response time, which was measured to be approximately 134 ms. This value surpasses that of other reported hydrogel-based sensors, such as the HPAAm/Chitosan-MWCNT hybrid sensor, which exhibited a response time of 180 ms and a recovery time of 151 ms.[45] This relatively short response time demonstrated the ability of the sensor to promptly detect changes in external pressure and translate them into electrical signals. The fast response was attributed to the high ion mobility within the hydrogel matrix and the close contact

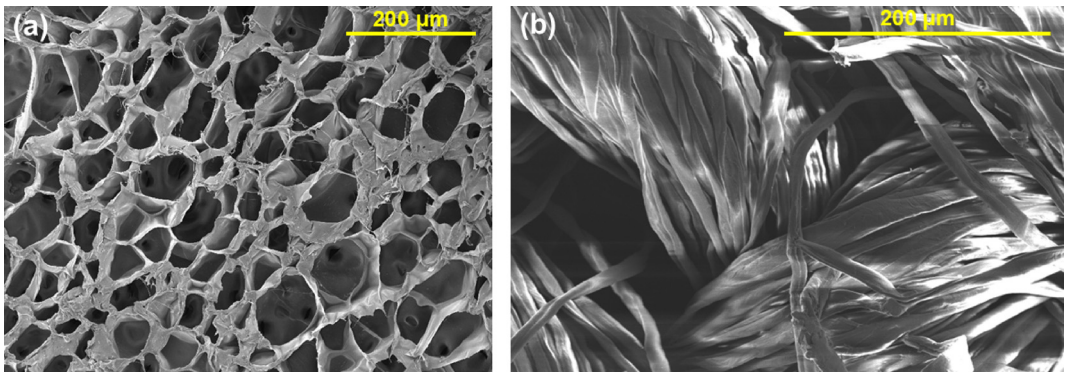

Fig. 2 (a) The microstructure of the PAAM–LiCl hydrogel; (b) untreated woven fabric.

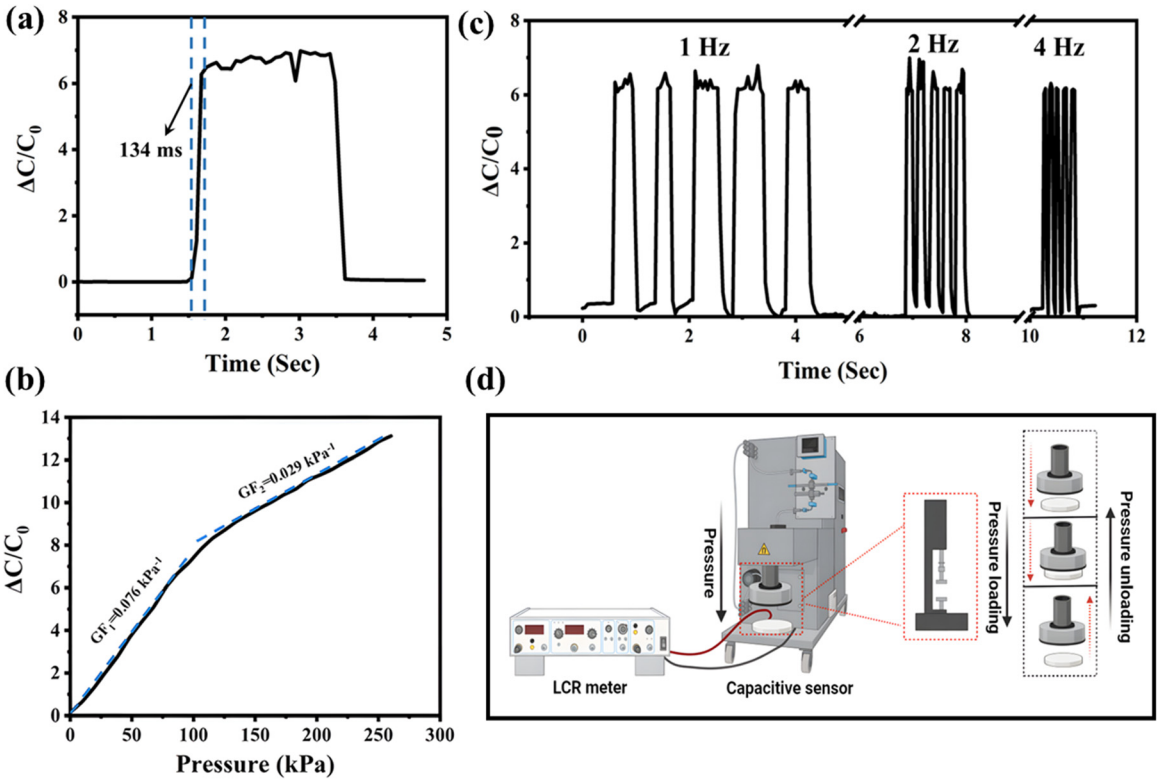

Fig. 3 Woven fabric-based ionic plain hydrogel pressure sensor: (a) response time with the woven electrode; (b) sensitivity of woven electrode; (c) same pressure and different frequency with the woven electrode; (d) system for capacitive pressure sensor testing, which pressure gauge is used to apply pressure, and the LCR meter is used to record the sensing data.

interface between the hydrogel and woven electrode. The open porous structure of the hydrogel facilitated rapid ionic redistribution under deformation, enabling quick dielectric modulation and measurable capacitance change.

4.2.2. Sensitivity and gauge factor (GF). To evaluate sensitivity, the relative capacitance change ($\Delta C/C_0$) was measured across a pressure range of 0–300 kPa, as shown in Fig. 3b. The curve reveals two distinct linear regions, each characterized by a different GF. In the low-pressure regime (0–100 kPa), the sensor exhibited a steeper slope with GF_1 = 0.076 kPa^{-1}, indicating high sensitivity to small pressures. By contrast, in the higher-pressure region (100–300 kPa), the slope decreased, yielding GF_2 = 0.029 kPa^{-1}, which reflects reduced sensitivity as the sensor approaches compressive saturation.

This dual-stage response can be explained by the evolution of the microporous network within the hydrogel under compression. At lower pressures, the interconnected micropores (50–200 μm) were progressively compressed, narrowing the spacing between ion-conducting channels. This compression enhances ion mobility and significantly alters the dielectric environment, producing pronounced capacitance changes and thus a higher GF. Once the pressure exceeds ~100 kPa, most pores have already collapsed, and further deformation arises primarily from the rearrangement of polymer chains within the dense hydrogel matrix. In this state, ion migration paths change only slightly, leading to a weaker capacitance response and the lower GF observed. Similar pore-to-chain dominated transitions have been reported in other hydrogel-based sensors by Ding *et al.*,[51] supporting this mechanistic interpretation.

The two-stage GF behavior therefore reflects a balance between pore compression–dominated sensitivity at low loads and polymer chain deformation–dominated stability at high loads. While the GF values were lower than those of the polyacrylamide–alginate hydrogel sensor reported by Ding *et al.* (GF = 0.91 kPa^{-1}), the present system demonstrates a broader pressure detection range (0–300 kPa) and reliable structural stability, highlighting its suitability for applications requiring both sensitivity and robustness.

4.2.3. Dynamic frequency response. The dynamic sensing performance of the fabricated device was systematically evaluated by subjecting it to periodic compressive pressures at frequencies of 1 Hz, 2 Hz, and 4 Hz while maintaining a constant loading amplitude, as illustrated in Fig. 3c. Across all frequencies, the sensor exhibited stable and well-defined $\Delta C/C_0$ peaks with consistent amplitude and spacing, indicating its capability to accurately follow rapid pressure variations without signal lag or distortion.

This high-frequency stability arises from the synergistic mechanical behavior of the fabric–hydrogel composite. The woven cotton substrate, composed of interlaced warp and weft yarns, provides a cross-locking architecture that distributes in-plane stress and effectively suppresses the accumulation of permanent deformation during repeated compression. The interwoven structure maintains dimensional integrity by

enabling slight lateral yarn displacement, which dissipates localized stress and prevents fatigue cracking. Simultaneously, the ionic hydrogel layer exhibited rapid elastic recovery and strong internal hydrogen bonding, allowing its microporous network to quickly return to its original configuration once the external load is removed. This rapid recovery re-establishes the ion-conducting pathways and dielectric spacing required for stable capacitance, thereby ensuring that each loading–unloading cycle produces a reproducible electrical response even at 4 Hz. The combination of fabric reinforcement and hydrogel elasticity, therefore, underpins the ability of the sensor to sustain repetitive, high-frequency pressure inputs without structural degradation or loss of signal fidelity, a property essential for real-time physiological monitoring and motion detection.

4.2.4. Sensor testing setup. The measurement system used for performance evaluation was illustrated in Fig. 3d. The woven hydrogel sensor was connected to an LCR meter, which recorded the capacitance changes in real-time. A mechanical force tester was employed to apply controlled compressive forces vertically onto the sensor surface. The sensor assembly included woven electrodes encapsulating the ionic hydrogel layer. This setup ensured consistent loading conditions, minimized environmental interference, and provided accurate measurements across multiple tests.

4.3. Stability and durability

The woven fabric-based hydrogel pressure sensor underwent a cyclic test, where woven electrodes were repetitively cycled from 0 to 10 000 repetitions (see Fig. 4a). This test aimed to assess the durability and stability of the sensor under repeated stress. The results confirmed excellent stability and durability, with consistent signal response throughout the entire cycling process. Such performance highlights the reliability and longevity of the sensor, which are critical factors for practical use.

The present durability evaluation was conducted under ambient laboratory conditions. However, to fully demonstrate the feasibility of continuous operation, it was essential to enhance the testing conditions by subjecting the sensor to extreme or fluctuating environments, such as elevated/low temperatures and varying humidity levels. Such assessments would provided deeper insights into the environmental tolerance and long-term operational stability of hydrogel-based sensors.

4.3.1. Gradient pressures for static and dynamic. The interaction between proximity and pressure sensing was also explored. The dynamic resistance response of the pressure sensor was measured for pressures from 30 kPa, 60 kPa, 80 kPa, 110 kPa, and 160 kPa (see Fig. 4b). The hydrogel sensor had relaxation cycles at a fixed maximum pressure (P = 160 kPa) for about 30 seconds. These values represent increasing levels of pressure applied to the system. By subjecting the system to these gradient pressures, it can study its response to varying stress levels. The behavior of the system under dynamic gradient pressures was essential for optimizing performance and reliability in real-world applications. The results from these experiments provided valuable insights into the sensitivity and adaptability of the sensor, which are vital for numerous scientific and engineering fields.

The experiment involved testing the hydrogel pressure sensor with gradient pressure values of 30 kPa, 60 kPa, 80 kPa, 110 kPa, and 160 kPa (see Fig. 4c). It exhibited the preeminent pressure-current response behavior of the hydrogel pressure sensor upon treatment with different pressures. To study the repeatability of detecting compressive strain or pressure, the

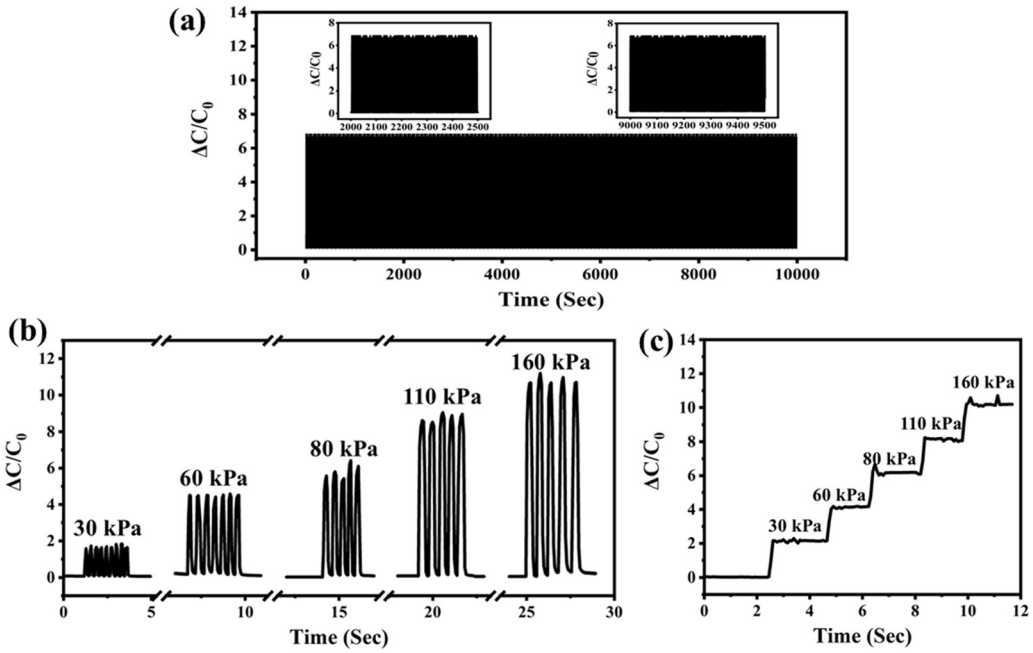

Fig. 4 Performance of woven fabric-based ionic plain hydrogel pressure sensor: (a) cycle for woven electrode; (b) gradient pressure for dynamic; (c) gradient pressure for static.

hydrogel sensor underwent relaxation cycles at a fixed maximum pressure (P = 160 kPa) for about 12 seconds. These values represent increasing levels of pressure applied to the sensor. The response of the sensor to these gradient pressures is static, providing insight into its sensitivity and ability to detect and measure pressure variations accurately. The data obtained from this experiment contributes to the scientific understanding of the capabilities of the sensor and aids in its effective implementation in practical scenarios.

4.4. Fourier transform infrared spectroscopy (FTIR)

The FTIR spectra of the plain hydrogel, woven fabric with plain hydrogel, and patterned hydrogel were analyzed to elucidate their chemical compositions and molecular interactions depicted in Fig. 5a. The plain hydrogel exhibited characteristic absorption bands at 3323 cm^{-1} and 1659 cm^{-1}, corresponding to O–H stretching vibrations (indicative of hydrogen-bonded water molecules) and C=O stretching vibrations (amide I band of polyacrylamide), respectively.[52] These findings confirmed the hydrophilic nature of the hydrogel and the presence of the polymer backbone. For the woven fabric with plain hydrogel, the spectrum revealed peaks at 3330 cm^{-1} (O–H stretching), 1664 cm^{-1} (C=O stretching, amide I), and 1014 cm^{-1} (C–O stretching of cellulose). The O–H and C=O peaks align with the structure of the hydrogel, while the 1014 cm^{-1} band confirmed the incorporation of cotton fabric, as cellulose-derived C–O bonds are prominent in cotton fibers.[53] The patterned hydrogel displayed similar functional groups, with O–H stretching at 3339 cm^{-1} and C=O stretching at 1655 cm^{-1}, reinforcing the consistency in hydrogel composition across different forms. The reference spectrum of woven cotton fabric exhibited distinct peaks at 1710 cm^{-1} (C=O stretching in cellulose) and 1017 cm^{-1} (C–O stretching), further validating the presence of cellulose in the composite material.[54] The slight shifts in wavenumbers between samples—such as the C=O stretching at 1655 cm^{-1} in the patterned hydrogel *versus* 1664 cm^{-1} in the composite—suggest microenvironmental variations, possibly due to differences in hydrogen bonding or polymer-fabric interactions. These results collectively demonstrated the successful integration of polyacrylamide hydrogel with cotton fabric, as evidenced by the retention of key functional groups in the composite. The FTIR analysis provided critical insights into the molecular structure of the hydrogels and their interactions with textile substrates, which is essential for optimizing their performance in potential biomedical or material applications.

4.5. Thermogravimetric analysis (TGA)

Thermogravimetric analysis (TGA) was performed to evaluate the thermal stability of plain hydrogel, woven fabric, and their composite (see Fig. 5b). The woven fabric exhibited a multi-step degradation profile, with an initial 3.2% weight loss at 260 °C due to moisture release, followed by a 27.27% loss at 370 °C attributed to hemicellulose and amorphous cellulose degradation, and a major 49.49% weight loss at 475 °C associated with the breakdown of crystalline cellulose.[55] In contrast, the plain hydrogel showed an early and significant 31.50% weight loss at 110 °C from free and bound water evaporation, followed by a 42.33% degradation at 490 °C linked to the decomposition of the polyacrylamide (PAAm) network and organic constituents.[56]

The composite structure presented a combined degradation behavior. An initial weight loss of 36.26% at 250 °C reflected simultaneous water loss from the hydrogel and partial decomposition of the fabric. This was followed by a pronounced 33.34% weight loss at 490 °C, which corresponds to the concurrent degradation of PAAm chains and cellulose, and a final 5.29% loss at 580 °C, suggesting residual carbonization. Notably, the main degradation peak of the composite (490 °C) was shifted to a higher temperature compared with the woven fabric (475 °C), highlighting improved thermal resistance.

This enhancement can be attributed to synergistic interfacial effects between the hydrogel and the fabric. The crystalline domains of cellulose act as rigid, thermally stable regions that physically confined the PAAm network, restricting chain mobility and delaying thermal scission. Simultaneously, the coordination between Li^+ ions and the amide groups of PAAm

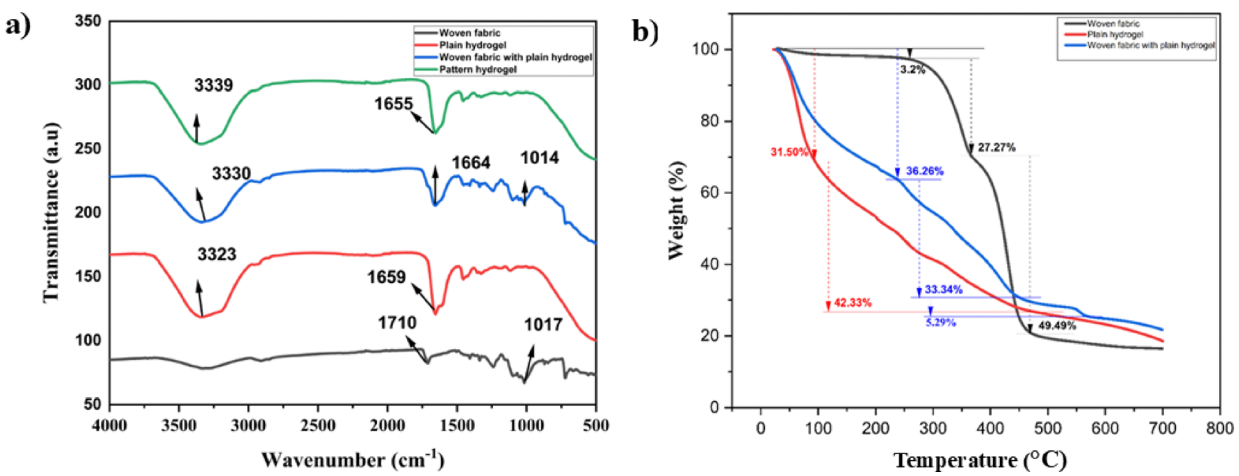

Fig. 5 (a) FTIR test for woven fabric with an ionic plain hydrogel; (b) TGA test for woven fabric with an ionic plain hydrogel.

introduces additional ionic crosslinking, which strengthens the polymer matrix and increases resistance to thermal decomposition. Together, these mechanisms—cellulose crystallinity providing physical restriction and Li^+–PAAm coordination contributing chemical stabilization—explain the observed elevation in degradation temperature of the composite relative to its individual components.

Therefore, the improved thermal stability arises not only from hydrogen bonding or generic interfacial interactions but from a dual mode of reinforcement: (i) structural confinement imposed by the crystalline cellulose framework of the woven fabric and (ii) ionic coordination within the PAAm–LiCl hydrogel. This cooperative effect ensures that the composite material combines the mechanical robustness of the fabric with the enhanced thermal resilience of the hydrogel, making it suitable for applications requiring durability under thermal stress.[57]

4.6. Self-adhesive performance of ionic plain hydrogel

The ionic plain hydrogel demonstrated remarkable self-adhesive performance across diverse material surfaces, including rubber, paper, plastic, metal, glass, wood, and textiles, as illustrated in Fig. 6. This versatile adhesion capability aligns with previous findings by Pang *et al.*,[58] where similar hydrogels exhibited strong bonding to glass, rubber, copper, and polypropylene while maintaining biocompatibility for skin applications. In our study, the hydrogel adhered effectively to rubber balls (a), paper cups (b), plastic bottles (c), aluminum scissors (d), plastic cups (e), tin clips (f), yarn bobbins (g), glass bottle caps (h), wooden cotton butts (i), and woven fabric (j), suggesting broad applicability in material science and biomedical engineering.[59] The adhesive mechanism likely stems from physical interactions—such as hydrogen bonding, van der Waals forces, and electrostatic attractions—between the polyacrylamide–LiCl network of the hydrogel and substrate surfaces. The incorporation of LiCl may enhance adhesion by modulating the ionic conductivity and interfacial energy of the hydrogel, thereby promoting stronger interfacial bonding.[60] Notably, the hydrogel-maintained adhesion under mechanical stress, indicating robust interfacial cohesion. This property is particularly advantageous for wearable devices, wound dressings, or flexible electronics, where reliable adhesion to heterogeneous surfaces is critical.[61] Future studies could quantify adhesion strength *via* peel or shear tests and explore correlations between LiCl concentration and adhesive performance. The results underscore the potential of ionic hydrogels as multifunctional, substrate-independent adhesives for industrial and biomedical applications.

4.7. Mechanical properties of plain and pattern hydrogel

The mechanical performance of plain and patterned polyacrylamide hydrogels were evaluated through tensile testing, revealing significant differences in their strain behavior despite being synthesized with identical chemical compositions (AAM monomer ratio, monomer concentration, and MBAA crosslinker quantity).[62] The sample dimensions before testing were total length 4cm, gauge length 2.9 cm, and thickness 0.5 cm (see Fig. 7c). The plain hydrogel demonstrated superior elongation capability, reaching a maximum tensile strain of 1046.72% (see Fig. 7a and d) with a peak stress of 0.38 MPa (see Fig. 7b), while the patterned hydrogel exhibited comparatively lower ductility, fracturing at 548.15% strain (Fig. 7a and e) under a similar stress of 0.39 MPa (see Fig. 7b). This divergence in mechanical behavior can be attributed to structural heterogeneities introduced during patterning—specifically, the alternating thick and thin regions in the patterned hydrogel act as stress concentrators, promoting localized deformation and premature failure.[63] In contrast, the uniform microstructure of the plain hydrogel facilitates more homogeneous stress distribution, enabling greater elongation before rupture. The near-identical peak stresses suggest that crosslinking density and polymer chain interactions remain consistent between the two variants, confirming that the observed mechanical differences arise solely from geometric design rather than material composition.[64] These findings highlight the critical role of structural engineering in hydrogel performance, where patterned architectures may sacrifice extensibility for tailored

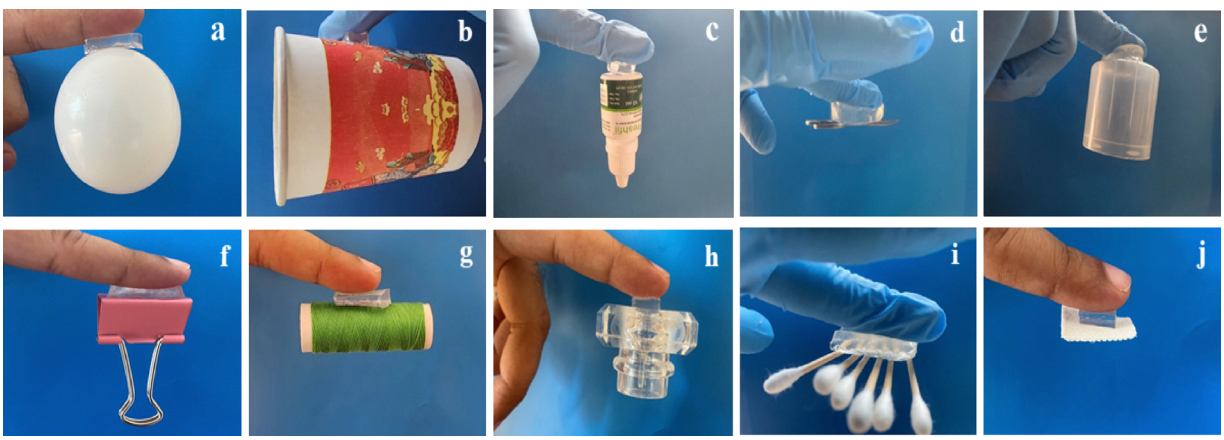

Fig. 6 The photos of polyacrylamide–LiCl ionic plain hydrogel adhere to different substrates. (a) Rubber ball; (b) paper cup; (c) plastic bottle; (d) aluminum scissors; (e) plastic cup; (f) Sn (tin) clip; (g) yarn bobbin; (h) glass made bottle cap; (i) wood made cotton butt; and (j) woven fabric.

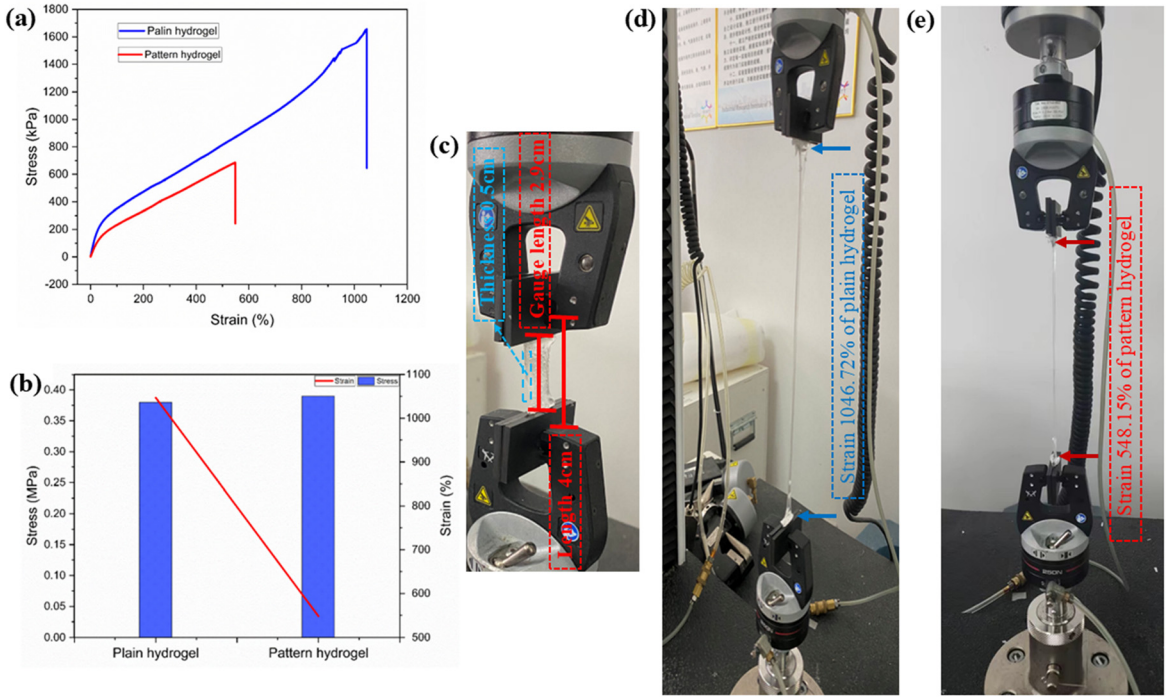

Fig. 7 The mechanical properties of plain and pattern hydrogel: (a) tensile stress; (b) tensile strain curves of the plain hydrogel and pattern hydrogel; (c) dimension of sample: total length 4 cm, gauge length 2.9 cm, and thickness 0.5 cm; (d) visual images of plain hydrogel strain; (e) visual images of pattern hydrogel strain.

functionality (*e.g.*, anisotropic responsiveness or fluidic channel integration). For applications requiring extreme deformability (*e.g.*, stretchable electronics or tissue scaffolds), plain hydrogels are preferable, whereas patterned designs could be optimized for controlled failure or directional mechanics.[65] Future work should explore hybrid architectures that balance structural complexity with mechanical resilience through computational modeling and advanced fabrication techniques.

4.8. Application on piano for sensing performance

Woven fabric electrodes used in a piano for sensing performance are an interesting topic that combines traditional musical instruments with modern technological advancements. The fabric can be used as a woven electrode in the keys or attached to specific areas of the instrument, allowing for precise and accurate sensing. This enables the capture of nuanced information, such as variations in key velocity, duration, and aftertouch, which are essential elements in creating expressive musical performances. Woven fabric electrode pressure sensors in pianos offer exciting opportunities to enhance the capabilities of the instrument, provide real-time feedback to performers, and enable new modes of interaction (see Fig. 8). By combining the rich history and tradition of the piano with the advancements in sensing technology, a new generation of instruments can be created to inspire musicians and push the boundaries of musical expression.

The presence of LiCl in the plain ionic hydrogel can influence the reaction by controlling the reaction conditions, such as temperature and ionic environment. This synthesis method allows for the controlled creation of a polymer with specific properties, making it valuable in various applications, including materials science, biotechnology, and drug delivery.

Fig. 8 Analysis of sensing performance using the piano of woven fabric electrode.

5. Conclusions

This research comprehensively investigated the development, characterization, and performance of a woven fabric-based plain hydrogel pressure sensor, showcasing its potential as a

flexible and durable candidate for pressure sensing applications. The fabrication process successfully integrated a plain hydrogel onto a woven fabric substrate, combining the mechanical flexibility of textiles with the sensitivity of hydrogels. Through systematic experimentation, key performance indicators were evaluated, including gauge factors (GF1 = 0.076 kPa^{-1}, and GF2 = 0.029 kPa^{-1}), a fast response time of 134 ms, and consistent performance under various dynamic frequencies (1 Hz, 2 Hz, and 4 Hz). Among the tested configurations, the sensor structure with GF1 demonstrated superior sensitivity, suggesting an optimized hydrogel-fabric interface that enhances electrical responsiveness to pressure changes. Durability tests confirmed outstanding mechanical robustness, with the sensor enduring over 10 000 loading-unloading cycles without significant performance loss, underscoring its long-term usability. FTIR analysis confirmed the presence of essential chemical bonds contributing to the hydrogel network, while TGA results revealed that both the plain hydrogel and its fabric-integrated counterpart maintained thermal stability up to 490 °C, highlighting their suitability for use in diverse thermal environments. Compared to conventional sensors, the woven fabric-based hydrogel sensor excels in flexibility, durability, and responsiveness, positioning it favorably for next-generation wearable and biomedical pressure-sensing technologies.

This study provides a solid foundation for advancing textile-integrated hydrogel sensors, which combine chemical, mechanical, and thermal performance in a single platform. Future research may focus on enhancing sensitivity through nanocomposite doping, miniaturization for wearable electronics, and integration into smart garments for real-time physiological monitoring. The convergence of hydrogel science and smart textiles opens promising avenues for practical applications in health diagnostics, human–machine interfaces, and soft robotics.

Authorship contributions

Conceptualization, T. M.; methodology, L. L., T. M. and M. H. K.; formal analysis, L. L., M. K., M. N. R., and X. R.; investigation, L. L., X. R., M. A. R., T. I., and M. K.; validation, L. L., M. N. R., X. R., and T. M.; resources, L. L., M. H. K., and T. M.; visualization, L. L., M. N. R., X. R., M. A. R., T. I., and M. K.; supervision, T. M.; original draft, L. L., M. H. K., and M. K.; writing, review and editing, L. L., M. K., M. N. R., X. R., T. I., T. M., and M. A. R.; All authors contributed to the article and approved the submitted version.

Conflicts of interest

The authors declared that they have no conflict of interest.

Data availability

The data will be available upon request from the corresponding authors.

Acknowledgements

This work was supported by the Key Research and Development Program of Shandong Province (2024CXGC010411), National Key Research and Development Program (2022YFB3805802), National Natural Science Foundation of China (52473307, 22208178, 62301290), Taishan Scholar Program of Shandong Province in China (tsqn202211116), Shandong Provincial Universities Youth Innovation Technology Plan Team (2023KJ223), Natural Science Foundation of Shandong Province of China (ZR2023YQ037, ZR2023QE043, ZR2022QE174, ZR2024ME012), Shandong Province Science and Technology Small and Medium sized Enterprise Innovation Ability Enhancement Project (2023TSGC0344, 2023TSGC1006), Natural Science Foundation of Qingdao (23-2-1-249-zyyd-jch, 24-4-4-zrjj-56-jch), China Postdoctoral Science Foundation (2024M761560), Anhui Province Postdoctoral Researcher Research Activity Funding Project (2023B706), Qingdao Key Technology Research and Industrialization Demonstration Projects (23-1-7-zdfn-2-hz), Qingdao Postdoctoral Funding Project (QDBSH20240201011), Suqian Key Research and Development Plan (H202310), and Systems Science Plus Joint Research Program of Qingdao University (XT2024202). The authors acknowledge the Department of Textile Engineering, Jashore University of Science and Technology, Bangladesh, for providing technical support.

References

1 M. A. R. Azady, S. Ahmed and M. S. Islam, *Eur. J. Chem.*, 2021, **12**, 329–339.
2 P. Sikdar, M. M. Uddin, T. M. Dip, S. Islam, M. S. Hoque, A. K. Dhar and S. Wu, *Mater. Adv.*, 2021, **2**, 4532–4573.
3 O. Wichterle and D. Lim, *Nature*, 1960, **185**, 117–118.
4 R. Eelkema and A. Pich, *Adv. Mater.*, 2020, **32**, 1906012.
5 L. Lu, S. Yuan, J. Wang, Y. Shen, S. Deng, L. Xie and Q. Yang, *Curr. Stem Cell Res. Ther.*, 2018, **13**, 490–496.
6 M. Rahman, M. Kabir, S. Chen and S. Wu, *Eur. Polym. J.*, 2023, **199**, 112480.
7 X. Liu, M. Gao, J. Chen, S. Guo, W. Zhu, L. Bai, W. Zhai, H. Du, H. Wu and C. Yan, *Adv. Funct. Mater.*, 2022, **32**, 2203323.
8 M. A. Mohamed, A. Fallahi, A. M. El-Sokkary, S. Salehi, M. A. Akl, A. Jafari, A. Tamayol, H. Fenniri, A. Khademhosseini and S. T. Andreadis, *Prog. Polym. Sci.*, 2019, **98**, 101147.
9 M. Rahman, M. Kabir, K. Li, Y. Li, S. Chen and S. Wu, *J. Mech. Behav. Biomed. Mater.*, 2024, 106769.
10 J. Yang, Y. Chen, L. Zhao, J. Zhang and H. Luo, *Polym. Rev.*, 2023, **63**, 574–612.
11 S. Bashir, M. Hina, J. Iqbal, A. Rajpar, M. Mujtaba, N. Alghamdi, S. Wageh, K. Ramesh and S. Ramesh, *Polymers*, 2020, **12**, 2702.
12 S. Shahi, H. Roghani-Mamaqani, S. Talebi and H. Mardani, *Coord. Chem. Rev.*, 2022, **455**, 214368.
13 X. Sun, F. Yao, C. Wang, Z. Qin, H. Zhang, Q. Yu, H. Zhang, X. Dong, Y. Wei and J. Li, *Macromol. Rapid Commun.*, 2020, **41**, 2000185.

14 C. Zhou, T. Wu, X. Xie, G. Song, X. Ma, Q. Mu, Z. Huang, X. Liu, C. Sun and W. Xu, *Eur. Polym. J.*, 2022, **177**, 111454.
15 J. Liu, W. Wang, H. Li, P. Huo, P. Teng, H. Ding and X. Shen, *Eur. Polym. J.*, 2024, 112895.
16 Q. Xu, Z. Wu, W. Zhao, M. He, N. Guo, L. Weng, Z. Lin, M. F. A. Taleb, M. M. Ibrahim and M. V. Singh, *Adv. Compos. Hybrid Mater.*, 2023, **6**, 203.
17 W.-Y. Guo and M.-G. Ma, *J. Mater. Chem. A*, 2024, **12**, 9371–9399.
18 L. Liza, M. H. Kabir, L. Jiang, S. Jerrams and S. Chen, *Sens. Diagn.*, 2023, **2**, 1414–1436.
19 M. S. B. Sadeque, H. K. Chowdhury, M. Rafique, M. A. Durmuş, M. K. Ahmed, M. M. Hasan, A. Erbaş, İ. Sarpkaya, F. Inci and M. Ordu, *J. Mater. Chem. C*, 2023, **11**, 9383–9424.
20 H. C. Ates, P. Q. Nguyen, L. Gonzalez-Macia, E. Morales-Narváez, F. Güder, J. J. Collins and C. Dincer, *Nat. Rev. Mater.*, 2022, **7**, 887–907.
21 L. Li, R. Sun, R. Zheng and Y. Huang, *Mater. Des.*, 2021, **205**, 109759.
22 B. Wang, S. Zhou, S. Jiang, S. Qin and B. Gao, *Anal. Chem.*, 2023, **95**, 8395–8410.
23 L. Kun, M. Kabir, M. Rahman and S. Chen, *Eur. Polym. J.*, 2025, 114251.
24 M. Xie, K. Hisano, M. Zhu, T. Toyoshi, M. Pan, S. Okada, O. Tsutsumi, S. Kawamura and C. Bowen, *Adv. Mater. Technol.*, 2019, **4**, 1800626.
25 Y. Zhang, X. Xia, K. Ma, G. Xia, M. Wu, Y. H. Cheung, H. Yu, B. Zou, X. Zhang and O. K. Farha, *Adv. Funct. Mater.*, 2023, **33**, 2301607.
26 A. Libanori, G. Chen, X. Zhao, Y. Zhou and J. Chen, *Nat. Electron.*, 2022, **5**, 142–156.
27 M. Mahinroosta, Z. J. Farsangi, A. Allahverdi and Z. Shakoori, *Mater. Today Chem.*, 2018, **8**, 42–55.
28 Z. Yin, H. Lu, L. Gan and Y. Zhang, *Adv. Mater. Technol.*, 2023, **8**, 2200654.
29 M. Kabir, M. K. Hasan, M. N. Rafi, M. R. Repon, T. Islam, J. Saha and M. Rahman, *ChemistrySelect*, 2024, **9**, e202403777.
30 S. Xian and M. J. Webber, *J. Mater. Chem. B*, 2020, **8**, 9197–9211.
31 T. Islam, S. M. Rasel, R. Roy, M. T. Hossen, S. Hossain, M. Rahman, M. Kabir, M. R. Repon, S. K. Maurya and M. Abdul Jalil, *Cellulose*, 2025, 1–13.
32 X. Ye, M. Tian, M. Li, H. Wang and Y. Shi, *Coatings*, 2022, **12**, 302.
33 X. Zhang, J. Chai, Y. Zhan, D. Cui, X. Wang and L. Gao, *Micromachines*, 2025, **16**, 330.
34 C. Dong, Y. Bai, J. Zou, J. Cheng, Y. An, Z. Zhang, Z. Li, S. Lin, S. Zhao and N. Li, *Nondestr. Test. Eval.*, 2024, **39**, 1749–1790.
35 L. Zhu, Y. Zhang, S. Chen, Z. Lin, Y. Zhang, X. Xie and Y. Qiao, *Chem. Eng. J.*, 2024, **497**, 154959.
36 J. Zhang, Y. Liang, Z. Deng, H. Xu, H. Zhang, B. Guo and J. Zhang, *ACS Appl. Mater. Interfaces*, 2023, **15**, 29902–29913.
37 Y. Wang, P. Chen, X. Zhou, Y. Liu, N. Wang and C. Gao, *ACS Appl. Mater. Interfaces*, 2022, **14**, 47100–47112.
38 M. Kabir, M. Rahman, T. Islam, Q. Meng, H. Liu, M. Li and S. Wu, *Chem. Eng. J.*, 2025, 162753.
39 T. Periyasamy, S. P. Asrafali and J. Lee, *Gels*, 2025, **11**, 372.
40 S. Mondal, S. Das and A. K. Nandi, *Soft Matter*, 2020, **16**, 1404–1454.
41 F. Ahmad, A. Nosheen, M. S. Atiq, B. Mushtaq, S. Ahmad, F. Azam, A. Rasheed and Y. Nawab, *Int. J. Biol. Macromol.*, 2024, **256**, 128422.
42 M. Rostamitabar, A. M. Abdelgawad, S. Jockenhoevel and S. Ghazanfari, *Macromol. Biosci.*, 2021, **21**, 2100021.
43 H. Morris and R. Murray, *Text. Prog.*, 2020, **52**, 1–127.
44 W. Li, J. Liu, J. Wei, Z. Yang, C. Ren and B. Li, *Adv. Funct. Mater.*, 2023, **33**, 2213485.
45 S. Xia, S. Song, F. Jia and G. Gao, *J. Mater. Chem. B*, 2019, **7**, 4638–4648.
46 K. J. De France, F. Xu and T. Hoare, *Adv. Healthcare Mater.*, 2018, **7**, 1700927.
47 Y. Liu, H. Wang and T. Zhong, *Cellulose*, 2025, **32**, 4815–4829.
48 S. Y. Li and H. Fu, *Cellulose*, 2021, **28**, 6739–6756.
49 D. R. King, T. L. Sun, Y. Huang, T. Kurokawa, T. Nonoyama, A. J. Crosby and J. P. Gong, *Mater. Horiz.*, 2015, **2**, 584–591.
50 L. Ma, H. Yang, W. Yu, M. Bai, L. Zhou, Z. Ren, H. Chen, L. Zhang, B. Xue and W. Sun, *Small*, 2025, **21**, 2501322.
51 H. Ding, Z. Wu, H. Wang, Z. Zhou, Y. Wei, K. Tao, X. Xie and J. Wu, *Mater. Horiz.*, 2022, **9**, 1935–1946.
52 L. Zhang, Q. Li, Y. Liang, G. Zhang, J. Zou, P. Fei and W. Lai, *Int. J. Biol. Macromol.*, 2024, **277**, 134351.
53 F. Ahmad, B. Mushtaq, F. A. Butt, M. S. Zafar, S. Ahmad, A. Afzal, Y. Nawab, A. Rasheed and Z. Ulker, *Polymers*, 2021, **13**, 4098.
54 J. Zhang, H. Yuan, L. Li, J. Zhang, M. Wang, Y. Le and J.-F. Chen, *ACS Sustainable Chem. Eng.*, 2022, **10**, 8172–8183.
55 M. N. Norizan, K. Abdan, M. S. Salit and R. Mohamed, *J. Phys. Sci.*, 2017, 28.
56 F. Cui, L. Xi, D. Wang, X. Tan, J. Li and T. Li, *ACS Appl. Mater. Interfaces*, 2023, **15**, 6035–6046.
57 J. Zhu, R. Wang, R. Geng, X. Zhang, F. Wang, T. Jiao, J. Yang, Z. Bai and Q. Peng, *RSC Adv.*, 2019, **9**, 22551–22558.
58 Q. Pang, H. Hu, H. Zhang, B. Qiao and L. Ma, *ACS Appl. Mater. Interfaces*, 2022, **14**, 26536–26547.
59 R. Li, J. Ren, M. Zhang, M. Li, Y. Li and W. Yang, *Biomacromolecules*, 2024, **25**, 614–625.
60 D. P. Dubal, N. R. Chodankar, D.-H. Kim and P. Gomez-Romero, *Chem. Soc. Rev.*, 2018, **47**, 2065–2129.
61 Q. Yu, Z. Zheng, X. Dong, R. Cao, S. Zhang, X. Wu and X. Zhang, *Soft Matter*, 2021, **17**, 8786–8804.
62 J. Yang, C.-R. Han, J.-F. Duan, M.-G. Ma, X.-M. Zhang, F. Xu and R.-C. Sun, *Cellulose*, 2013, **20**, 227–237.
63 W. Xing and Y. Tang, *Nano Mater. Sci.*, 2022, **4**, 83–96.
64 E. Olaret, S. I. Voicu, R. Oprea, F. Miculescu, L. Butac, I.-C. Stancu and A. Serafim, *Polymers*, 2022, **14**, 2320.
65 M. L. Oyen, *Int. Mater. Rev.*, 2014, **59**, 44–59.